ELSEVIER

Journal of Nuclear Materials 241–243 (1997) 135–148

journal of nuclear materials

Island divertor studies on W7-AS

F. Sardei [a,*], Y. Feng [a], P. Grigull [a], G. Herre [a], D. Hildebrandt [b], J.V. Hofmann [a], J. Kisslinger [a], R. Brakel [a], J. Das [a], J. Geiger [a], O. Heinrich [a], G. Kühner [a], H. Niedermeyer [a], D. Reiter [c], M. Richter-Glötzl [a], A. Runov [d], R. Schneider [a], U. Stroth [a], H. Verbeek [a], F. Wagner [a], R. Wolf [a], W7-AS Team [a], NBI Group [a]

[a] *Max-Planck-Institut für Plasmaphysik, EURATOM Ass., D-85748 Garching, Germany*
[b] *Max-Planck-Institut für Plasmaphysik, EURATOM Ass., D-10117 Berlin, Germany*
[c] *Institut für Plasmaphysik, Forschungszentrum Jülich GmbH, EURATOM-KFA Ass., D-52425 Jülich, Germany*
[d] *RRC 'Kurchatov Institute', Moscow, Russia*

Abstract

Basic topological features of the island divertor concept for low shear stellarators are discussed with emphasis on the differences to tokamak divertors. Extensive measurements of the edge structures by two-dimensional plasma spectroscopy and by target calorimetry are in excellent agreement with predicted vacuum and equilibrium configurations, which are available up to central β values of $\sim 1\%$. For this β value the calculated field-line pitch inside the islands is twice that of the corresponding vacuum case. Video observations of the strike points indicate stability of the island structures for central β values up to $\sim 3.7\%$. The interpretation of the complex island divertor physics of W7-AS has become possible by the development of the three-dimensional plasma transport code EMC3 (Edge Monte Carlo 3D), which has been coupled self-consistently to the EIRENE neutral gas code. Analysis of high density NBI discharges gives strong indications of stable high recycling conditions for $\bar{n}_e \geq 10^{20}$ m^{-3}. The observations are reproduced by the EMC3/EIRENE code and supported by calculations with the B2/EIRENE code adapted to W7-AS. Improvement of recycling, pumping and target load distribution is expected from the new optimized target plates and baffles to be installed in W7-AS.

Keywords: W7-AS; Divertor plasma; 3D model; Plasma density diagnostic; Plasma temperature diagnostic

1. Introduction

In the past five years, increasing theoretical effort has been devoted to the exploration and optimization of suitable divertor concepts for low shear stellarators [1–3]. The interest in the island divertor approach is largely motivated by the favorable diversion properties of the stellarator boundary in the presence of large 'natural' magnetic islands (Section 2) and by the high geometric flexibility of such configurations. The island divertor concept can as well be applied to high shear helical systems like CHS and LHD. In CHS, a local island divertor (LID) has been installed in order to demonstrate its basic function and its efficiency in view of its future use in the LHD device [4]. The LID concept, however, is based on a single $m/n = 1/1$ edge island generated by field perturbation coils located above and below the torus. Externally induced magnetic perturbations are also used to provide divertor action in the ergodic divertor of TORE SUPRA, which exploits a large stochastic boundary layer to reduce the target power load, extend the radiation zone and improve particle control and impurity screening [5].

The W7-AS 'high ι' configurations, bounded by natural islands of considerable size, have the basic properties required for an island divertor. The target arrangement installed presently (see Section 4), is the first step on the way to an optimized divertor, which will start operation within the next two years. Fig. 1 shows the plasma column

* Corresponding author. Tel.: +49-89 3299 1389; fax: +49-89 3299 2584; e-mail: sardei@ipp-garching.mpg.de.

PII S0022-3115(96)00501-6

and the optimized target plates and baffles for the proposed W7-AS and W7-X divertors. Note the similarity of both configurations concerning aspect ratio and field periodicity as well as inherent 3-dimensionality of plasma and plasma facing structures. The present and the next step of the divertor development in W7-AS are intended to provide first experimental experience on divertor operation in a low-shear stellarator. In particular, they are aimed to clarify to what extent the vacuum edge structures are modified by plasma pressure, whether high recycling conditions similar to those of tokamak divertors can be achieved, and whether stellarator specific solutions will emerge for the exhaust problem. Extrapolability to W7-X is not obvious, although some of the key edge parameters of W7-AS, as the radial island width and the power flux density across the separatrix, are comparable to those of W7-X. Owing to the complexity of the island topology and the strong toroidal inhomogeneity of the recycling processes, the development of three-dimensional transport models is a prerequisite for reliable prediction of the plasma behaviour and realistic interpretation of the experimental data.

After reviewing the basic features of the island divertor concept for low shear stellarators and the basic differences to tokamak divertors, this paper describes the experimental and modelling investigations on island divertor configurations of Wendelstein 7-AS during the past year. Section 2 introduces 'natural islands' as inherent diverting structures

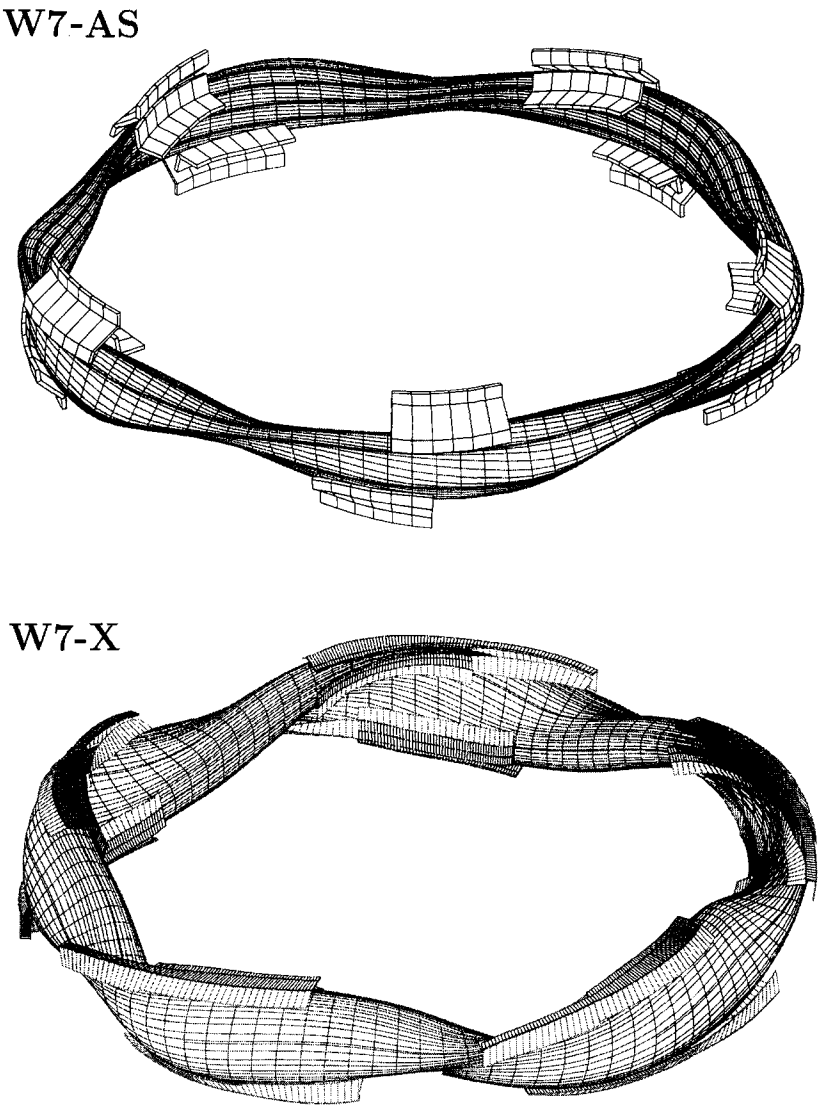

Fig. 1. Plasma column and divertor target and baffle arrangement of W7-AS ($R = 2$ m) and W7-X ($R = 5.5$ m). Note the discontinuous divertor elements compared to tokamak divertors.

of low shear stellarators, for which flux coordinates exist or can be derived, at least for all divertor-relevant configurations of W7-AS. Section 3 addresses basic properties of the island divertor related to the island topology and the toroidal inhomogeneities of plasma and targets and their consequences for plasma recycling and transport. A detailed comparison of measured and predicted edge structures for vacuum and moderate-β configurations is presented in Section 4. Section 5 briefly describes the models used for transport investigations on W7-AS, namely the B2/EIRENE code adapted to the toroidally averaged island geometry of W7-AS and a new 3D code, EMC3/EIRENE, developed to simulate and interpret the experiments. In Section 6, results from a transport analysis of NBI discharges for different line-averaged densities are discussed and compared to simulations with the EMC3/EIRENE code. Section 7 gives a short outlook into the new optimized island divertor for W7-AS.

2. Natural islands in W7-AS

In island divertors of low shear stellarators as well as in tokamak divertors, the field lines outside the last closed flux surface (LCFS) are diverted to target plates. However, in the first case the diverted field lines form nested island surfaces surrounding completely the LCFS (Fig. 2). The plasma diffusing across the LCFS enters the island regions and is directed to the target plates located at the rear of the islands. The islands originate at resonances of sideband Fourier harmonics B_{mn} of the radial B spectrum with the local values of the rotational transform $t = M_{\mathrm{per}} m/n$ (M_{per} = number of field periods). These harmonics reflect the inherent non-axisymmetry of the configuration and the properties of the modular coils. Typically, the largest islands occur at lowest-order resonances $m = 1$ ($t = 5/n$ for W7-AS and W7-X) and appear at the edge. The poloidal and radial width of the islands scale as a/n and $\sqrt{B_{mn}/(t'n)}$ [6], respectively, with t' the magnetic shear at a, the radial position of the island chain. Although shear increases towards the edge, there is generally only one low-order island chain governing the relevant boundary region. In W7-AS, the configuration with the 5/9 islands at the edge offers a good compromise between large plasma and large island size, and therefore has been chosen for standard divertor operation. Fig. 2 shows the islands in the 'triangular' and 'elliptical' cross sections (symmetry planes). Depending on the t profile, the islands may be topologically closed or 'open'. In the first case (Fig. 2), standard flux coordinates are available for the islands and can be used for mapping experimental data and for defining a 3D modelling grid. If the edge t value is slightly decreased with respect to this case, the island chain is shifted outside and the island flux surfaces eventually break up beginning at the separatrix (open island case). What is left finally is a chain of strongly diverted island fragments, regularly distributed according to the poloidal mode number of the island resonance. These regular structures can be represented by nested 'open magnetic surfaces', spanned by field lines, for which generalized flux coordinates can be obtained [7]. This procedure provides a mapping framework for all open edge configurations of W7-AS in the t range relevant for divertor operation.

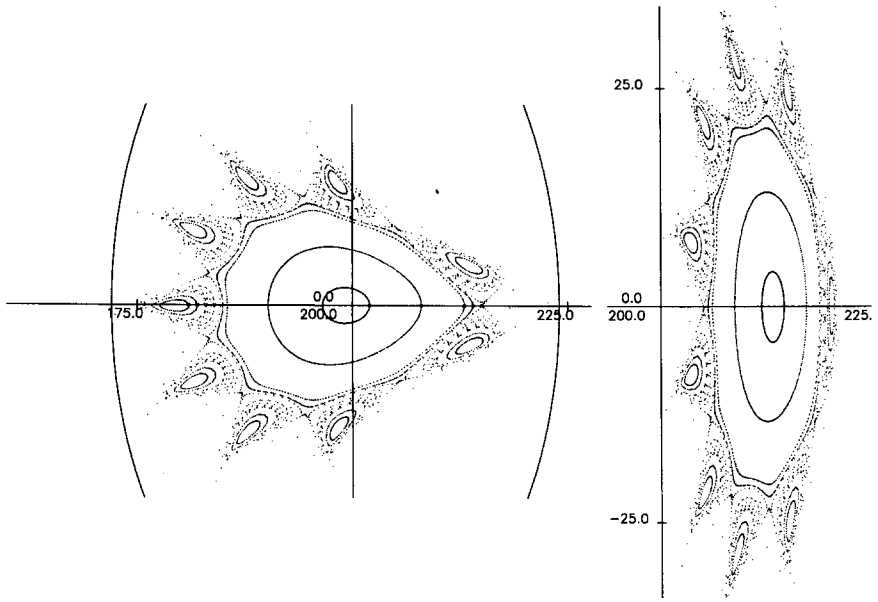

Fig. 2. 'Natural' island chain of the $t = 5/9$ resonance in the 'triangular' and 'elliptical' cross sections of W7-AS.

3. Island divertor versus tokamak divertor

Unlike in tokamak divertors, the X-lines in island divertors are helical, with the pitch given by the resonant t of the island chain. The poloidal progression of the field lines in the island reference frame is a measure of the internal rotational transform inside the island, t_i, and determines the connection length, L_c, from target to target. As in tokamaks, the SOL extends poloidally from the stagnation point via X-point down to the targets (Fig. 3). However, the island SOL is poloidally closed in front of the targets, which enables trapping of recycling particles. The short distance between the targets and the LCFS (~ 5 cm for W7-AS and ~ 8 cm for W7-X, standard configuration), requires higher plasma densities than in comparable tokamaks to effectively decouple the recycling neutrals and the target-released impurities from the plasma core. On the other hand, recycling inside the island tends to raise the local density and hence improves the screening of neutrals and impurities. This effect is illustrated schematically in Fig. 4. If the main plasma density is small (upper drawing), ionization takes place in the main plasma and the density drops from the separatrix into the island (island low recycling). Increasing the plasma density shifts the ionization into the island (lower drawing), and the trapped particles lead to a density rise inside the island (island high recycling).

The efficiency of this process depends strongly on the distance of the targets from the LCFS and on L_c, i.e. on the radial position, radial width and internal field-line pitch of the islands. These quantities can be optimized by varying t, the vertical field or the currents of control loops [8], which change the radial and poloidal field components. L_c has a crucial impact on the divertor performance, as it directly affects the ratio of parallel to radial power transport to the targets. Small values of L_c imply small temperature decay lengths, λ_T, which favors a parallel thermal coupling between the main plasma and the targets and a recycling close to the outer separatrices (tokamak divertor case). On the other hand, large values of L_c favor a cross-island thermal coupling, which, in the extreme case, removes the divertor action, so that limiter conditions are

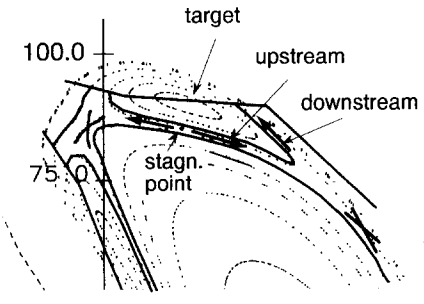

Fig. 3. Upstream and downstream SOL of a magnetic island intersected by a target plate.

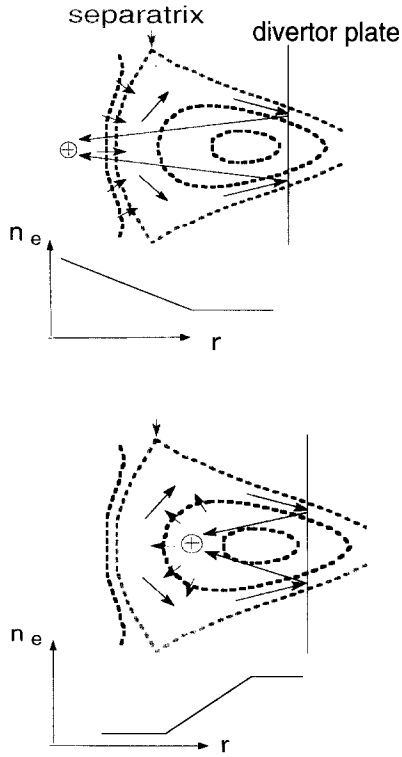

Fig. 4. Principle of low (top) and high (bottom) recycling inside islands intersected by target plates.

approached. If parallel and cross-island heat transport are in balance, then an extended recycling and high-density zone can be established inside the islands, while maintaining the diverting property of the islands (island divertor recycling). This balance requires λ_T to be comparable with the average radial extension of the island region intersected by the target plates:

$$\lambda_T/\delta = \tfrac{7}{4} L_c \sqrt{\alpha \chi_\perp n_{up} / \left(\kappa_0 T_{up}^{5/2}\right)} \,/\delta \approx 1,$$

where the subscript 'up' indicates upstream conditions and $\alpha \equiv L_X/L_c\,(1 - 0.5 L_X/L_c)$, with L_X/L_c being the fraction of the connection length facing the main plasma. The expression for λ_T is derived from the solution of simplified momentum balance and heat conduction equations [9], by assuming n to be radially constant over λ_T and the power into the SOL evenly distributed over L_X. Application to the highest density case analyzed in this study (see Section 6), with $L_c = 160$ m, $L_X/L_c = 0.7$ and $\delta = 5$ cm, yields $\lambda_T/\delta = 0.45$, indicating a significant, but not dominant thermal coupling across the islands. Correcting for the real island geometry would slightly increase the heat penetration length. Realistic L_c values are 100 to 300 m for W7-AS and W7-X. These values also satisfy the requirement of a large temperature drop along the field lines for high density discharges [10].

The poloidal width of the islands, i.e. the distance between the two divertor fans, is ~ 5 cm (in the average) for the 5/9 resonance of W7-AS. Since the two fans carry particles flowing in opposite directions, the relatively small radial scale length may induce strong anomalous shear viscosity inside the islands, contributing significantly to

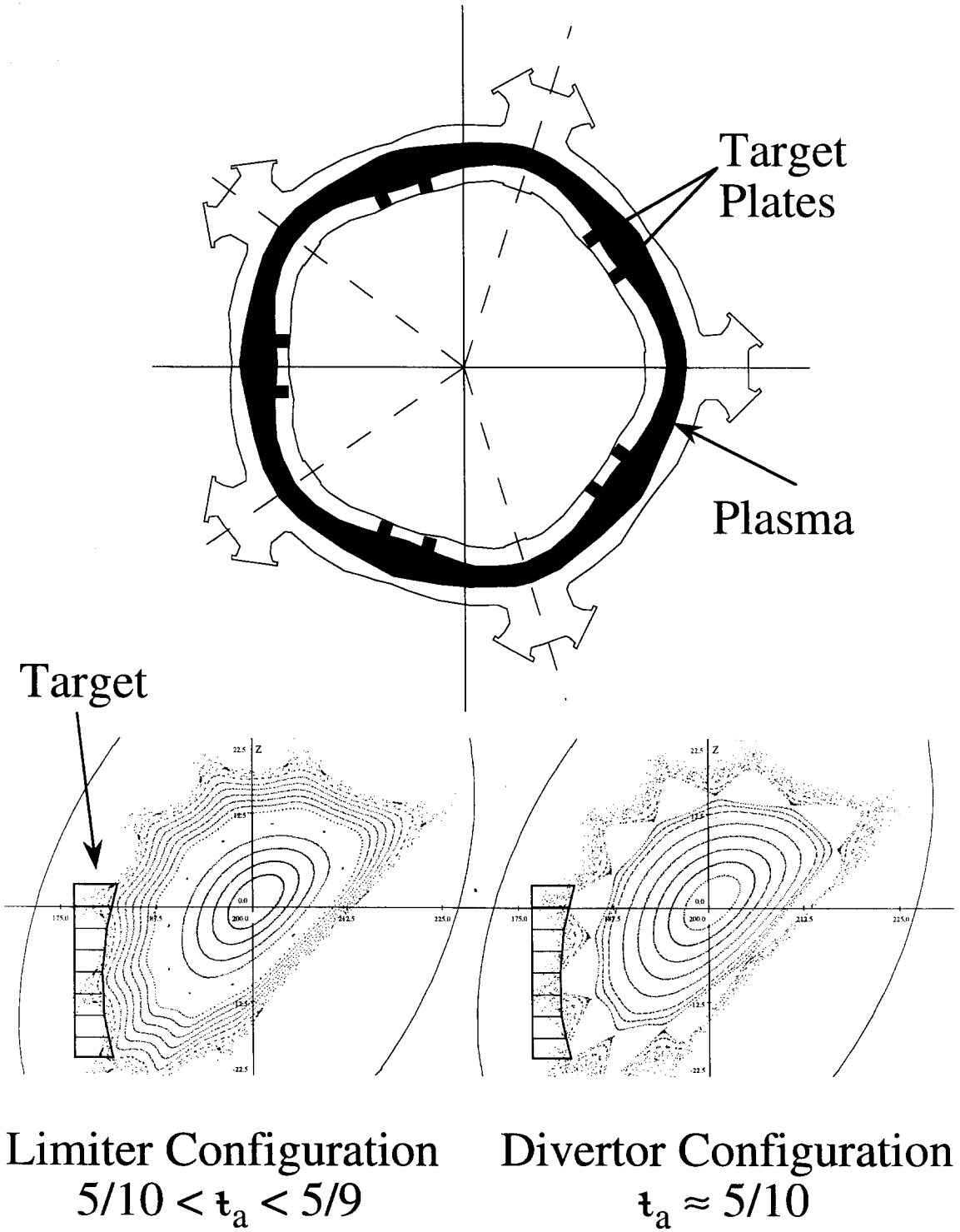

Fig. 5. Present target plate arrangement in W7-AS.

the total parallel momentum losses. This effect is not known in tokamaks.

A second basic geometric difference is the intrinsic three-dimensionality of island divertors. Besides the toroidal variation of the island shape, which leads to higher radial coupling of the flux tubes at positions of smaller radial width, a parallel modulation of the plasma parameters is introduced by the discontinuous target plates [11,12]. This is due to the local strong periodic interaction of the outflowing plasma with the recycling neutrals and target-released impurities. (Note that the total wetted target length is $\sim 1/18$ of the total island length for W7-AS (optimized divertor) and $\sim 1/10$ for W7-X (Fig. 1). This modulation is superimposed to the standard parallel gradients associated with the heat conduction to the target plates. It cannot be removed by parallel heat conduction for downstream temperatures $T < 10$ eV. Here, an adequate toroidal resolution of diagnostics and modelling is required. Furthermore, discontinuous target plates must be tilted toroidally with respect to the field lines in order to avoid leading edges arising from poloidal progression of the field lines, poloidal diffusion or poloidal drift motion. The tilt determines the toroidal length of the target plates and hence the target load density.

Both the peaking of the density inside the islands for high recycling conditions and the parallel modulation of the plasma parameter profiles due to discontinuous target plates have been predicted by the new 3D Monte Carlo edge transport code EMC3 (see Section 5), applied to the optimized W7-AS target plates (see Section 7) [11,12].

4. Edge topology

As a first step towards an island divertor for W7-AS, the previous two up/down rail limiters have been replaced by a set of 10 inboard target plates (segmented CFC graphite blocks of 23 cm poloidal and 12 cm toroidal size each). The plates are placed toroidally on both sides of the triangular cross sections (Fig. 5) and preserve both the inherent fivefold periodicity and up/down symmetry of the configuration. Both limiter and divertor operation are possible, depending on whether the target plates intersect regular flux surfaces or islands (Fig. 5). For divertor operation with a given edge resonance $t_a = 5/n$ (Fig. 5), the inboard position of the targets allows an easy variation of the connection lengths by application of a vertical field shifting the configuration horizontally with respect to the targets.

Extensive experimental investigations have been carried out in order to check the reliability of the predicted island structures and their geometric integrity against β effects. These are prerequisites for a successful island divertor operation and for a realistic use of transport models based on predicted topology. Fig. 6 compares measured and calculated edge structures for a $t_a \sim 5/8$ configuration at low β (central $\beta_0 = 0.25\%$). The video image (right picture) is a tangential view through ~ 2.5 m of the plasma column in the light of carbon (CIII, 467 nm). With an ionization potential of 48 eV, this species resides in a small radial shell close to the LCFS. The contours shown in the left hand side of Fig. 6 visualize successive

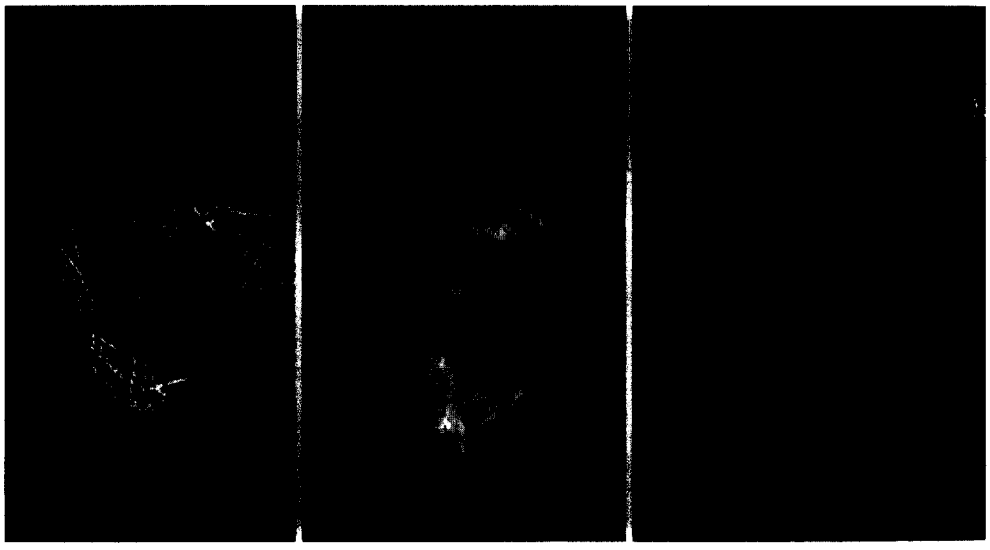

Fig. 6. Measured (video image of CIII, right picture) and calculated (left and central pictures) W7-AS edge structures for a $t = 5/8$ resonance. The calculated contour and density plots are perspective views of a single flux surface close to the LCFS.

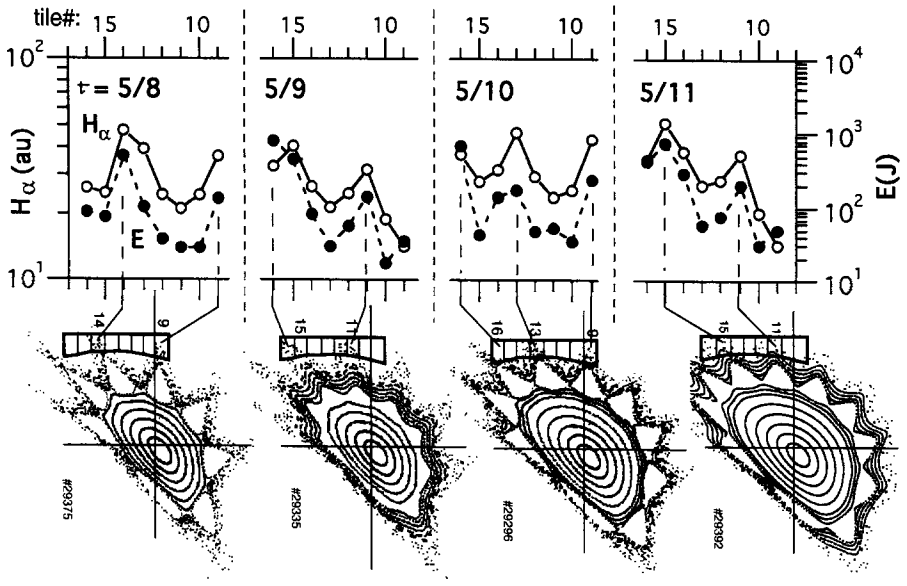

Fig. 7. Particle flux (H_α) and energy deposition (target calorimetry) profiles on a target plate for different edge resonances. The profiles peak at the intersections of the corrugated island boundary with the target.

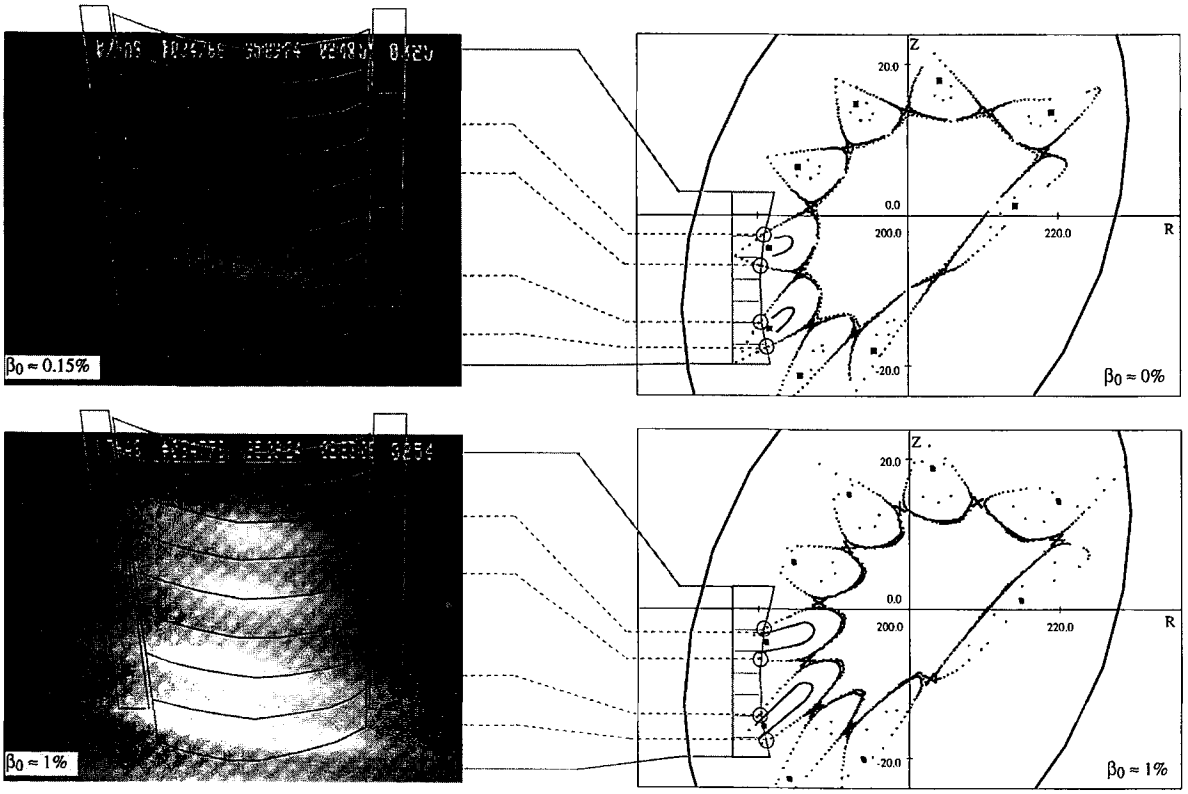

Fig. 8. H_α view (video) of the strike points of the 5/9 island fans for low and moderate beta values (left) and corresponding Poincaré plots of vacuum and equilibrium calculations (right). The island surfaces remain intact and the strike points stable against β effects.

poloidal cross sections of a single vacuum flux surface next to the LCFS in a perspective projection as seen by the video camera. The most prominent cross section at $\phi = 17°$ is emphasized by a bold contour. The central picture results from the perspective projection of the flux surface itself, weighted with a constant density distribution. All relevant features of the video picture, including the multiple structures at the bottom and at the inboard (left) side, are reproduced by the simulations. The excellent agreement can be regarded as a three-dimensional verification of the edge structures close to the inner separatrix of the 5/8 vacuum island chain.

Experimental evidence of the edge structures close to the outer separatrix of the 5/8–5/11 vacuum island chains is provided by the flux of the recycling particles (H_α light) and by the heat load (target calorimetry) across the 8 tiles of a target plate (Fig. 7). The islands are well defined and closed, the target plates have limiter function and no divertor action is expected in these cases. The maxima of the profiles clearly appear at the intersections of the corrugated island boundary with the target. The minima reflect the usual radial decay of the plasma parameters in a limiter SOL. The phase shift of the island position between resonances with even and odd poloidal mode numbers is well reproduced by the experimental profiles. The discrepancy in the amplitude factor of the H_α profile modulation with respect to that of the heat load is mainly due to (a) the temperature decay in the limiter SOL, (b) the deviation of the ionization to the H_α emission rate at low temperatures and (c) the poloidal spread of the neutral fluxes.

If, however, the islands are intersected by the targets, divertor fans are formed along the outer island separatrices. The island chains shown in the Poincaré plots of Fig. 8 refer to vacuum and $\beta_0 = 1\%$ conditions, respectively, with the same external currents, corresponding to $t_a \approx 5/9$ configurations. The $\beta_0 = 1\%$ configuration was obtained with the KW equilibrium code [13]. (Higher-β equilibrium calculations are not available at present.) It shows an increased radial elongation of the islands due to field modifications from the internal plasma currents. The most relevant change, however, is the doubling of the field-line pitch inside the islands, which reduces the connection length to half of its value. The island surfaces remain intact and their phases unchanged. This is confirmed by the video pictures of Fig. 8, showing the island strike points via H_α light emission of recycling particles. (The 8 tiles of the target are visualized in an overlay to the video picture.) For both configurations, the locations of the observed H_α stripes on the target coincide very accurately with the predicted strike points shown on the right, proving the reliability of the calculated equilibrium edge configuration. $\beta_0 = 1\%$ is slightly below the highest β value of the discharges analyzed in the present study (Section 6). However, the structure and phase of the observed poloidal stripe sequence are found to be stable up to $\beta_0 \sim 3.7\%$, corresponding to $\langle \beta \rangle \sim 1.8\%$. This demonstrates the robustness of the 5/9 islands for divertor-relevant applications.

5. Transport models

Sophisticated 2D plasma transport codes, coupled with Monte Carlo codes for the neutral gas, are widely used in tokamak divertors to interpret experimental data, improve the basic understanding of plasma and impurity behaviour and predict and optimize the performance of new divertors [14–16]. In island divertors, additional effects introduced by the island topology and the toroidal target discretization (see Section 3) complicate the description of the divertor physics compared to tokamaks, motivating the urgent need of adequate 3D models. In the present study, the plasma edge transport of W7-AS was modelled with the B2 code [17,18] and the EMC3 (Edge Monte Carlo 3D) code, which was developed recently for island divertors [11,12]. Both codes are coupled with the EIRENE code [19] for the neutral transport. The chosen 5/9 edge configuration is described by three distinct sets of Fourier coefficients representing the island chain and the adjacent flux surfaces at the radial inside and outside of the islands (Fig. 9b). The islands are intersected by the targets outside the 0-points. In the B2 code, a 2D grid is obtained by helical averaging of islands and targets (over 9 field periods), which results in a single island configuration, bounded by the target, two private flux regions and the main plasma (Fig. 9a). The code requires an orthogonal grid, which can be realized only approximately in W7-AS. Even with these restrictions, the B2/EIRENE code can be used to estimate basic effects of the island geometry on the divertor physics in all regimes and to provide 2D reference solutions and benchmarks for the EMC3 code.

The EMC3 code is a fully selfconsistent 3D Monte Carlo code which solves, in a first step, a simplified version of the 3D time-independent plasma fluid equations. The main assumptions of the present first version of the code are single fluid plasma, neglect of heat convection and parametrization of momentum losses from experimental data. All diffusive terms are treated by following Monte Carlo particles in magnetic coordinates. Islands, private flux region and target plates are modelled in their real 3D geometry (see Fig. 9b, showing the grid at the cross section of the targets). High flexibility for resolving strongly diverted magnetic structures and high gradients near the targets is provided by a locally (3D) adjustable, non-orthogonal grid. The 3D particle, momentum and energy transport equations, coupled with the EIRENE code for the neutral gas, are solved iteratively in sequence. Particle and energy sources from EIRENE code are included in the transport equations. Standard Bohm conditions are assumed at the target plates. D, $\chi_\perp$, $n_{e,sep}$ (plasma density at the LCFS), P_{sep} (power flux across the

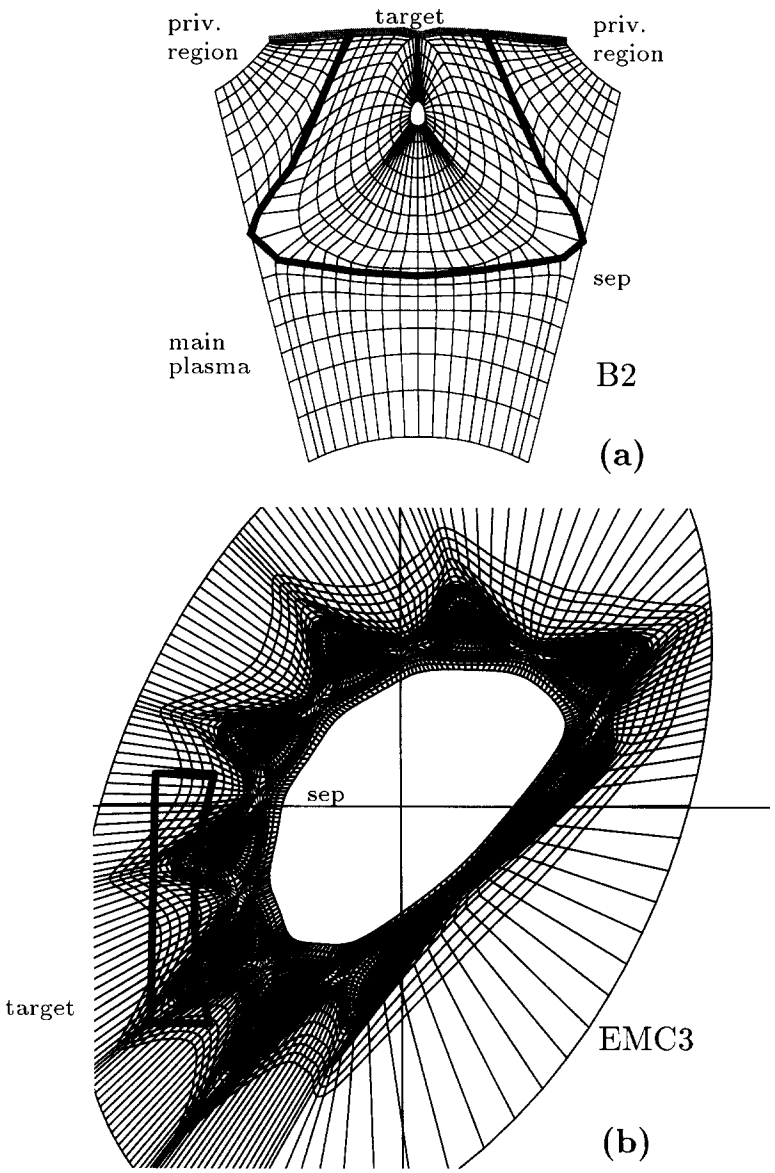

Fig. 9. 2D grid used in the B2 code and 3D grid used in the EMC3 code for a 5/9 island divertor configuration. The 3D grid is shown at the cross section of the targets.

LCFS) and α (total parallel momentum loss parameter) are input quantities obtained from experimental data. In the present study, P_{sep} was taken from the NBI power deposition after subtracting the plasma core radiation (estimated from Soft-X and bolometer data) and $\chi_{\perp}$ was set equal $3^{*}D$, according to previous estimations from density scans at $t = 0.34$. The remaining three parameters were chosen so as to match Langmuir probe data at upstream and downstream positions [20]. Parallelization of the EMC3/EIRENE code is under way.

Since B2 describes sophisticated physics in a simplified (2D) geometry, whereas EMC3 describes simplified physics in a sophisticated (3D) geometry, the two codes are of complementary use for island divertor investigations on W7-AS.

6. Transport results

The EMC3/EIRENE code was first applied to the planned optimized island divertor of W7-AS, for which it predicted high recycling conditions associated with a strong density rise inside the islands [11,12]. The results have motivated extensive experimental studies aimed to clarify

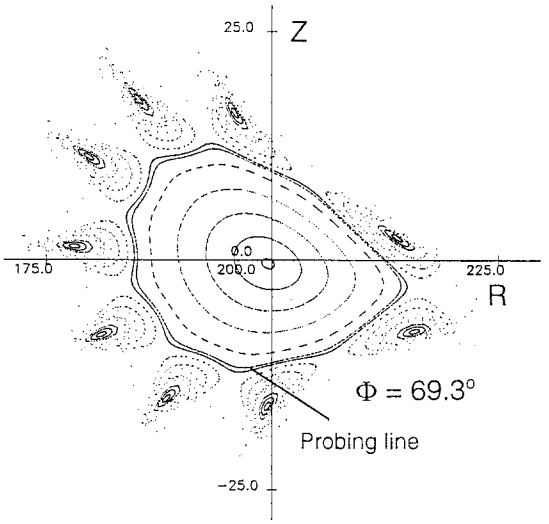

Fig. 10. Path across an island of the fast-reciprocating Langmuir probe used for comparison of measured and calculated density profiles.

whether the predicted high recycling regime can be obtained with the present inboard target plates. The analysis was performed on net-current compensated NBI discharges at $B = 2.5T$ with ECRH start-up and balanced injection. The configuration was defined by the edge iota parameter $t_a = 0.564$, which corresponds to a 5/9 island chain intersected by the targets outside the O-point (see Section 5), with a β corrected target-to-target connection length of $L_c \approx 160$ m. Line-averaged densities $\bar{n}_e$ were varied between 0.2 and 1.5 10^{20} m^{-3}. Heating powers were 0.8 MW for $\bar{n}_e \leq 0.8 \times 10^{20}$ m^{-3} and 2 MW for $\bar{n}_e = 1.2 \times 10^{20}$ m^{-3}. A central β value of $\sim 1.2\%$ was estimated for the 2 MW discharges. The data for the analysis were obtained during flat top phases of about 300 ms (low to moderate densities) or 150–200 ms (highest densities). In the latter case, density control was lost after that time and the discharges were terminated softly by radiative collapse. n_e and T_e data were provided by two Langmuir probes: a fast-reciprocating probe (FRLP) crossing an island at a position far from the target (Fig. 10) and a second probe close to the target. The measurements were supplemented by Thomson scattering, spectroscopy (H_α diode arrays looking at the targets, CCD cameras for H_α and CIII radiation), bolometry, low energy CX neutral analysis (LENA) and target thermography.

The results for the density range mentioned above are summarized in Figs. 11 and 12. Fig. 11a shows density profiles along the path of the FRLP across the island (Fig. 10), and the respective results from the EMC3/EIRENE code. Indicated in the picture are also the island-bounding inner and outer separatrices and the two points per profile, where the code results are matched to the experiments. (A third matching point is located at the downstream probe close to the target (see Ref. [20] for details)). Thomson scattering data are also shown for reference. The measured density profiles are rather flat except for the highest $\bar{n}_e$, for which the density peaks close to the outer separatrix. In all cases the profiles are well reproduced by the code. For $\bar{n}_e \leq 8 \times 10^{19}$ m^{-3}, the diffusion coefficient resulting from the modelling (after adjusting the input parameters to the experiment) is 0.6 m^2/s, dropping to 0.2 m^2/s for the highest density. These values are smaller than those resulting from the scaling derived for limiter configuration without boundary islands [21].

The corresponding measured and simulated temperature profiles for the highest and lowest $\bar{n}_e$ are shown in Fig. 11b. The higher temperatures predicted for the first case may be ascribed to the missing impurity radiation in the code.

Fig. 12 shows upstream and downstream densities and temperatures for the same discharges as functions of $\bar{n}_e$. At $\bar{n}_e \sim 10^{20}$, abrupt steepening of the downstream density (up to three times the upstream value), of the flux amplifi-

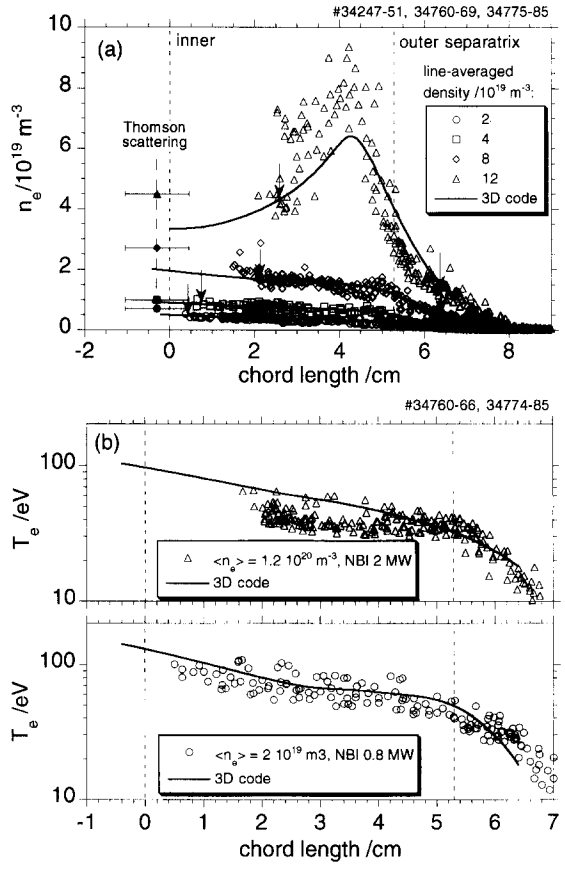

Fig. 11. (a): Measured and calculated density profiles along the probing path shown in Fig. 10 and Thomson scattering data. (b): Temperature profiles for the highest and lowest line-averaged densities shown in (a).

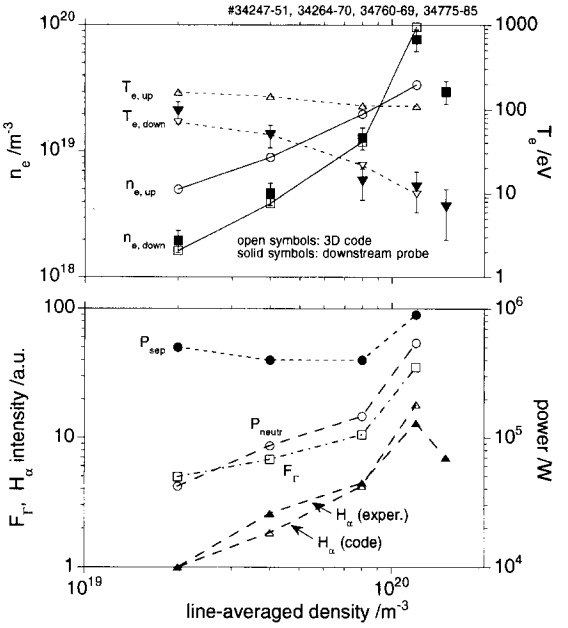

Fig. 12. Upstream and downstream densities, neutral power loss, flux amplification factor and H_α from experimental and code data as function of the line-averaged density. Rollover of density and H_α at the highest densities indicate detachment.

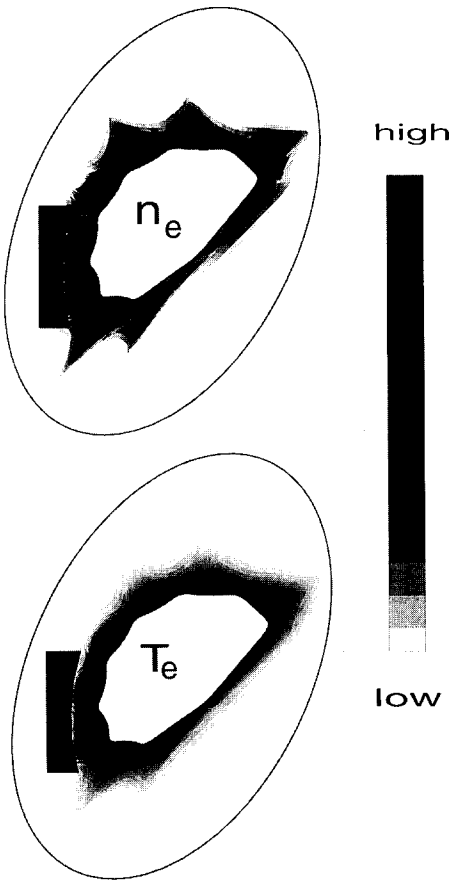

Fig. 13. Two-dimensional plot of the calculated density and temperature for the high density case shown in Fig. 11.

cation factor (up to 35) and of the measured and calculated H_α is shown, whereas the downstream temperature drops to about 10 eV and the total neutral power losses rise to ~ 50% of the power crossing the LCFS. Furthermore, the CX spectra of the escaping neutrals from LENA (not shown here) shift to much smaller mean energies. All these results together give experimental evidence of high recycling conditions for $\bar{n}_e \geq 10^{20}$ m^{-3}. At the highest densities shown in Fig. 12, $\bar{n}_e = 1.5 \times 10^{20}$ m^{-3}, the measured downstream density and H_α drop again, indicating detachment. This interpretation is supported by several additional observations from the plasma boundary [20]:

- The maximum of the Langmuir probe density profile is shifted inwards.
- The CIII radiation from the targets (tangential video view) is shifted towards the X-point, indicating a shrinking of the plasma column.
- The H_α radiation at the targets (radial video view) is strongly reduced and its modulation across the targets (H_α stripes at the strike points, see Section 4) disappears.
- The total target load (from thermography) decreases below 10% of the heating power.

However, density control was generally lost at that time and the discharges terminated in a radiative collapse. Fig. 12 also shows a significant pressure drop even for low densities, for which momentum loss by CX with neutrals cannot contribute significantly. This is probably due to anomalous radial transport of parallel momentum due to the combined effects of shear viscosity related to the small island size of W7-AS (see Section 3), and radial particle diffusion into the private flux region [18]. The 2D distribution of density and temperature in the triangular cross

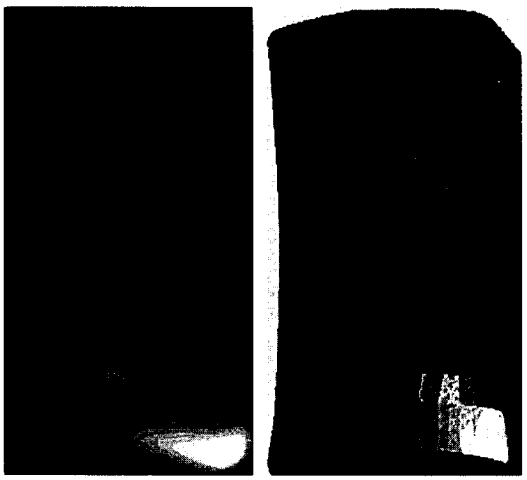

Fig. 14. Typical thermal load distribution over the target plates from thermography (left) and 3D heat flux calculations (right).

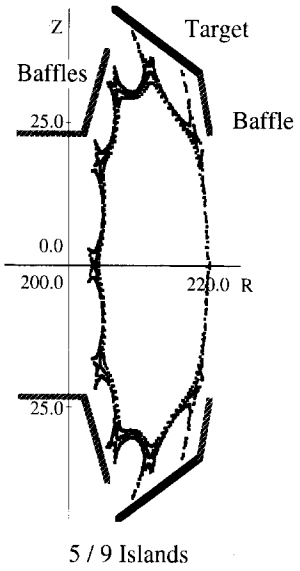

Fig. 15. Cross-section of the optimized island divertor arrangement for W7-AS (see also Fig. 1).

section, obtained with the EMC3/EIRENE code for the $\bar{n}_e = 1.2 \times 10^{20}$ m^{-3} case, is visualized in Fig. 13.

The thermal load on the target plates, as resulting from target thermography and EMC3/EIRENE heat flux calculations, is not homogeneous (Fig. 14), indicating strong localization of the heat fluxes along the island fan with the largest connection length, which collects a large power fraction crossing the LCFS. This island fan corresponds to the strike point located at largest distance from the midplane (see, for example, bottom strike point in Fig. 8). The connection lengths to the other strike points is much smaller due to mutual shading of the upper and lower target plates.

7. New optimized divertor for W7-AS

Improved divertor performance in W7-AS is expected from the planned additional control coils and optimized target plates and baffles [2]. Very small field perturbations ($\sim 10^{-4}$ of the main field) introduced by the additional current loops will be sufficient to modify significantly the island size and position, as well as the connection length. This will increase the flexibility of divertor operation. The new 10 target plates (Fig. 1) will be placed symmetrically at the top and bottom of the elliptical cross sections (Fig. 15), where the islands have their largest radial extent and their largest distance from the magnetic axis. Homogeneously wetted target areas and a careful avoidance of leading edges will provide recycling fluxes focussing predominantly into the islands. For the new divertor, the

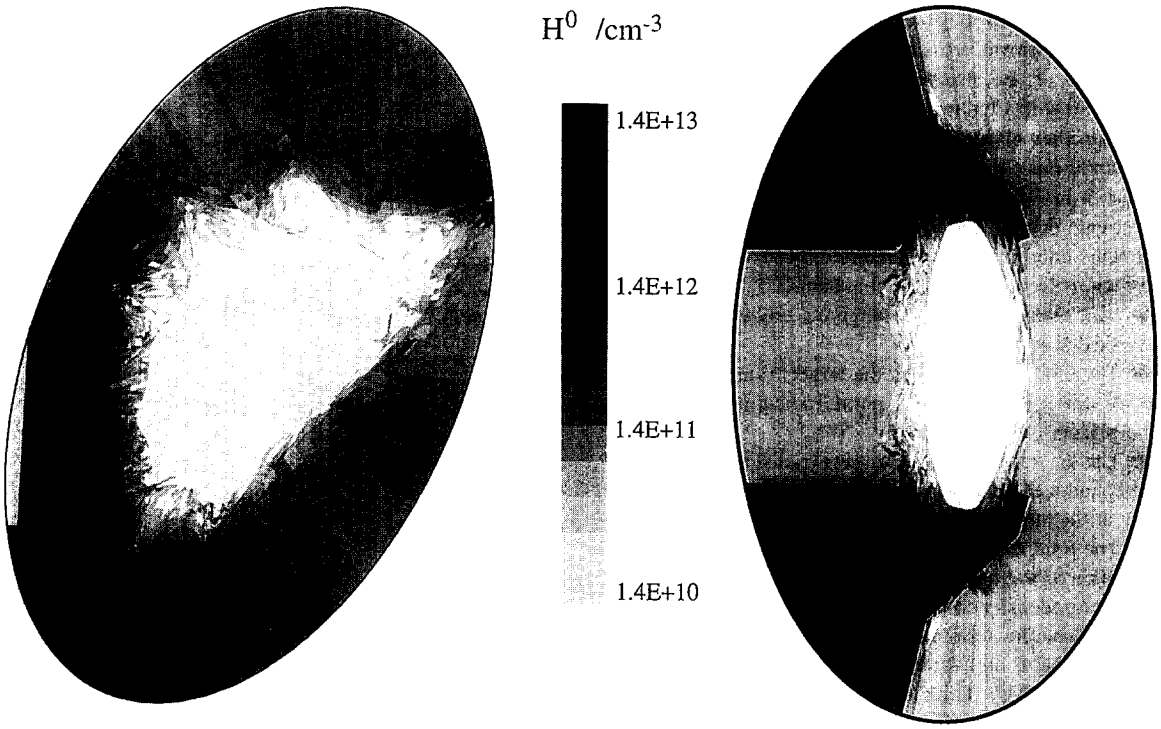

Fig. 16. Typical two-dimensionl neutral density distributions in the poloidal plane of the present (left) and optimized (right) target plates for W7-AS.

EMC3/EIRENE code calculations predict the onset of high recycling at lower densities than for the present target arrangement. Furthermore, neutral compression due to target inclination and baffles leads to neutral densities in the divertor chamber more than two orders of magnitude higher than outside of it, in contrast to the poloidally widespread distribution of the neutrals predicted for the present targets (Fig. 16).

8. Summary and conclusions

Different from tokamak divertors, the edge topology of island divertors in low shear stellarators is intrinsically three-dimensional. Edge resonance, island size and position and connection length are variable quantities, which can be optimized by varying t, B_z and the currents of control coils. Discontinous target plates imply a toroidal localization of recycling, which leads to locally higher densities and improved neutral screening from the main plasma, thus compensating, to a certain extent, for the shorter distance between the target plates and the main plasma. Strong radial shear viscosity contributing to significant parallel momentum losses may arise by friction between particles flowing in opposite direction along the island fans, which are very close to each other in W7-AS. The target load is generally two-dimensional, and diagnostics and modelling of the low temperature downstream plasma need adequate parallel resolution.

The vacuum edge corrugations due to the $5/n$ resonances are reflected with high accuracy in tangential video pictures and particle and energy deposition profiles over the target plates. For islands intersected by the target plates, equilibrium calculations up to $\beta_0 = 1\%$ accurately reproduce the strike points of the island fans, as visualized by H_α (video) profiles over a target plate. The equilibrium currents increase the field-line pitch inside the islands, which, for $\beta_0 = 1\%$, becomes twice as large as that of the vacuum field. This implies shorter connection lengths, which have to be taken into account in the transport modelling. The observed H_α stripe sequences are stable over a central β range up to $\beta_0 \sim 3.7\%$.

3D transport modelling has been shown to be essential for the interpretation of island divertor experiments. The new EMC3 transport code, coupled selfconsistently with the EIRENE code, has been applied to the interpretation of a high recycling 3D island divertor plasma. In the present version of the code, the parallel momentum losses are not yet included explicitely, but they are parametrized from experimental data.

Experimental evidence of high recycling conditions for $\bar{n}_e \geq 10^{20}$ m^{-3} and 1 MW power across the separatrix is indicated by peaking of the density inside the islands and close to the targets as well as by steepening of target-H_α emission as function of $\bar{n}_e$. For $\bar{n}_e = 1.2 \times 10^{20}$ m^{-3}, the flux amplification factor becomes 35 and the downstream density rises to three times that of the upstream value, as deduced from the EMC3/EIRENE code simulations. The parallel pressure drop is relatively high even for low line-averaged densities, indicating a significant contribution from radial shear viscosity. For highest line-averaged densities of 1.5×10^{20} m^{-3}, the downstream density decreases again, suggesting rollover consistent with detachment. The probe density profiles and the H_α profiles on the targets are reproduced satisfactorily by the EMC3/EIRENE code simulations. For the same discharges the B2/EIRENE code, adapted to W7-AS by helically averaging islands and targets, indicates onset of high recycling at lower upstream densities, which is probably due to the assumed toroidal and poloidal symmetry of the idealized targets in the code. Experiments with improved density control (by combined NBI and ECR heating) are planned in order to assess the feasibility of a stable detached plasma regime for both the present and the next divertor arrangements.

The new W7-AS divertor will be optimized with respect to target position, load distribution, recycling and pumping efficiency. Compared to the present targets, the EMC3 code predicts, for the new divertor, a stronger neutral compression near the targets. Ionization will be focussed inside the islands, leading to higher densities there and at the target plates for the same upstream density and input power. This also implies a transition from low to high recycling at lower upstream densities.

For W7-X and larger stellarators, the increasing size of the islands will reduce the plasma flux to the targets due to cross-field transport, the penetration of the neutrals into the plasma core and the momentum transfer across the islands by radial shear viscosity. That is, within the toroidal range of the targets the island divertor physics will become closer to 2D tokamak-like conditions, except for the confining effects of closed islands. However, all positive and negative implications of toroidal plasma inhomogeneity and discontinuous targets will remain.

References

[1] J. Nührenberg, E. Strumberger, D. Sünder and D. Reiter, Proc. 14th IAEA Int. Conf. Würzburg 1992, Plasma Physics and Contr. Nucl. Fusion Res., Vol. 2, Vienna (1993) p. 449.
[2] C.D. Beidler et al., 9th Int. Conf. Stellarators, Garching, Germany 1993, Rep. IAEA, Vienna (1993) p. 385.
[3] J. Kisslinger et al., 21st Eur. Conf. Contr. Fusion Plasma Phys., Montpellier, France (1994) ECA 18B, I, p. 368.
[4] A. Komori et al., these Proceedings, p. 967.
[5] Ph. Ghendrih et al., Topical Review, Plasma Phys. Contr. Fusion, submitted.
[6] M.N. Rosenbluth et al., Nucl. Fusion 6 (1966) 297.
[7] F. Sardei et al., Contrib. Plasma Phys. 34 (1994) 113.
[8] P. Merkel and J. Kisslinger, 19th Eur. Conf. Contr. Fusion Plasma Phys. Innsbruck, Austria (1992) ECA 16C, I, p. 587.

[9] K. Borrass, Nucl. Fusion 31 (1991) 1035.
[10] P.C. Stangeby and G.M. McCracken, Nucl. Fusion 30 (1990) 1225.
[11] Y. Feng, F. Sardei, J. Kisslinger and P. Grigull, these Proceedings, p. 930.
[12] F. Sardei et al., Contrib. Plasma Phys. 36 (1996) 166.
[13] J. Kisslinger, H. Wobig, 12th Eur. Conf. Contr. Fusion Plasma Phys. Budapest, Hungary (1985) ECA 9F, I, p. 453.
[14] A. Loarte, these Proceedings, p. 118.
[15] R. Schneider et al., J. Nucl. Mater. 196–198 (1992) 810.
[16] M.E. Fenstermacher et al., J. Nucl. Mater. 220–222 (1995) 330.
[17] B.J. Braams, Report (NET) EUR-FU/XII-8 = /87/68, Comm. EC, Brussels (1987).
[18] G. Herre, R. Schneider, D. Coster, F. Sardei, D. Reiter, P. Grigull and J. Kisslinger, these Proceedings, p. 941.
[19] D. Reiter, J. Nucl. Mater. 196–198 (1992) 80.
[20] P. Grigull et al., these Proceedings, p. 935.
[21] P. Grigull et al., 10th Int. Conf. Stellarators, IAEA Technical Meeting, Madrid, Spain, Rep. EUR-CIEMAT 30 (1995) 73.